# On-line indirect thermal measurement in a radiant furnace by a reduced modal model

Benjamin Gaume, Yassine Rouizi, Frédéric Joly, Olivier Quéméner

Version of Record: https://www.sciencedirect.com/science/article/pii/S0017931021007845
Manuscript_6ab6741818be500fc15ab4a1135393a5

# On-line indirect thermal measurement in a radiant furnace by a reduced modal model

B. Gaume*, Y. Rouizi, F. Joly, O. Quéméner

*LMEE, Univ Evry, Université Paris-Saclay, 91020, Evry, France.*

## Abstract

We propose an original method to recover the whole thermal field of a heated object on a furnace from a few measurement points. The radiant thermal source is first identified via a low order reduced model based on AROMM (Amalgam Reduced Order Modal Model) method. From this identified temperature, the thermal field is then recovered by direct simulation using a reduced model of higher order which leads to a better precision. This process is applied to a complex titanium object heated by two radiant panels placed in the furnace. From two measurement points, the temperature of the heated object is recovered on-line, with a mean error below $3\,K$.

*Keywords:* `Inverse Problem, Thermal Radiation, Reduced Modal Model, Radiosity Method, Industrial Furnace`

*Corresponding author. Tel.:+33 1 69 47 79 36
*Email address:* `b.gaume@iut.univ-evry.fr` (B. Gaume)

*Preprint submitted to International Journal of Heat and Mass Transfer*

## 1. Introduction

Inverse problem is a situation where the cause is deduced from the consequences. This thematic has been the subject of numerous works in the domain of conductive heat transfer. It is an ill-posed problem, and as such is often solved by iterative procedures, which are time-consuming by nature. As the temperature increases, heat transfer by radiation becomes significant and has to be modeled rigorously. The inherent complexity of radiative heat transfer leads to intricate numerical models which, combined with an iterative inverse procedure, results in unbearable computation time. Thus, as revealed by the literature, geometric complexity remains trivial when compared to a realistic industrial installation.

The most general modeling considers radiation trough semi-transparent media, able to absorb and emit their own heat flux in all directions. The number of degrees of freedom (DoF) explodes, as the thermal scene has to be meshed in its entirety and as the number of variables needed to represent the physics increases. Thus, whatever the considered models and the resolutions schemes, inverse problems stays limited to simple 2D configurations [1, 2].

Nevertheless, a whole range of high temperature thermal problems does not necessitate such complex models, as the media is either air, which can be viewed as a non-participating media, or even vacuum, in aerospace applications for example. For such problems, only the solid parts of the scene have to be meshed. First works concerning inverse radiative problems appeared in the 2000s. Conduction was neglected and radiative heat flux was computed by the radiosity method. In general, the thermal characteristics of a heating surface were recovered from the ones of a target surface. The entire panel of inverse techniques has been tested for 2D configurations [3, 4]. From the 2010s, more sophisticated works related on furnace design. The position and the power delivered by radiant panels were optimized in order to satisfy objectives on a heated object [5, 6, 7, 8, 9].

With the same radiative modeling, Farahmand *et al.* [10] performed a shape optimization of an enclosure from the knowledge of a source and a target, in order to satisfy a desired temperature and heat flux. In the aerospace domain, the problem of the aging of the protective materials of a spacecraft has been addressed in [11]. Global radiative properties (absorption coefficient and emissivity) were identified using a simplified discrete thermal model which considers the inertia of the materials and all of the external thermal stresses according to a given trajectory of the spacecraft. Some authors also focused on diffuse spectral models, in which thermal characteristics depends on the wavelength. Bayat *et al.* for example used a conjugate gradient method to identify the power emitted by a radiant panel from the temperature of a target [12].

Inverse problems involving combined heat transfers have also been investigated. The coupling of radiative heat transfer with natural convection in a bi-dimensional cavity has been proposed in [13]. Radiative heat transfer has also been coupled with conduction in [14]: Thermal properties of a 1D wall have been recovered in the context of space studies. Finally, Dehghani *et al.* [15] identified the temperature of a wall from temperature measurements of a heated piece, in a geometry made of two rectangles.

To overcome the computational difficulty engendered by complex geometries, reduced models can be employed. In particular, modal methods maintain the integrity of the geometry while decreasing the number of DoF necessary to describe the problem. Temperature is searched as a weighted sum of a limited number of spatial functions known in advance. Thermal problem resolution reduces to the computation of the weighting coefficients (also referred to as excitation states). The Modal Identification Method has been used to solve inverse heat conduction problems [16, 17]. Recently Girault *et al.* [18] have extended this method to radiative heat transfer to identify thermophysical parameters of semi-transparent grey media for an axi-symmetric geometry. In a similar way, Proper Orthogonal Decomposition has been applied to inverse problem involving radiation in semi-transparent media. Park *et al.* identified radiative properties of gas [19], heat sources [20] or the heat transfer coefficient between a gas and its surrounding wall [21]. Using Single Value Decomposition, a diffuse spectral model in a 3D geometry has been considered in [22].

The approach adopted in the present paper is the Amalgam Reduced Order Modal Model (AROMM) [23, 24]. In previous works [25, 26, 27], the interest of this method for solving inverse heat conduction problems has been established, especially when they are characterized by a complex geometry requiring a large number of nodes and/or a real time identification target. Particularly, the reduced base is independent of the boundary conditions, and time-dependent exchange coefficient has been considered. This independence towards boundary conditions makes this method appropriate for radiative dominated problems. In this context, Gaume *et al.* [28] combine AROMM and radiosity methods to solve direct problem within a complex geometry placed in a non-participating media. The authors showed that the resulting reduced model induces an important gain in terms of computation time, while allowing the reconstruction of the whole temperature field with a satisfying precision. Thus, AROMM method can be an adequate tool for inverse problems where radiation and conduction are involved.

The objective of the present work is to use AROMM method to recover the temperature of radiant panels of an industrial furnace from a few measurements, and from there, by taking advantage of the modal formulation, to deduce the entire thermal field of the scene. A technique is thus obtained that allows on-line monitoring of the heating of an object, whatever its geometry. The paper is organized as follows: the studied configuration is presented in section 2, and the modal formulation in section 3. Section 4 is dedicated to the inverse formulation applied to modal formalism. Finally, results are discussed in section 5. Section 6 offers a conclusion to the paper.

## 2. Problem position

### *2.1. Physical configuration*

An industrial furnace with thin walls is considered (Fig. 1). The heated object is characterized by a footprint (overall dimensions) of $0.4 \times 0.4 \times 1\,m^3$.The insulation is modeled via a low value

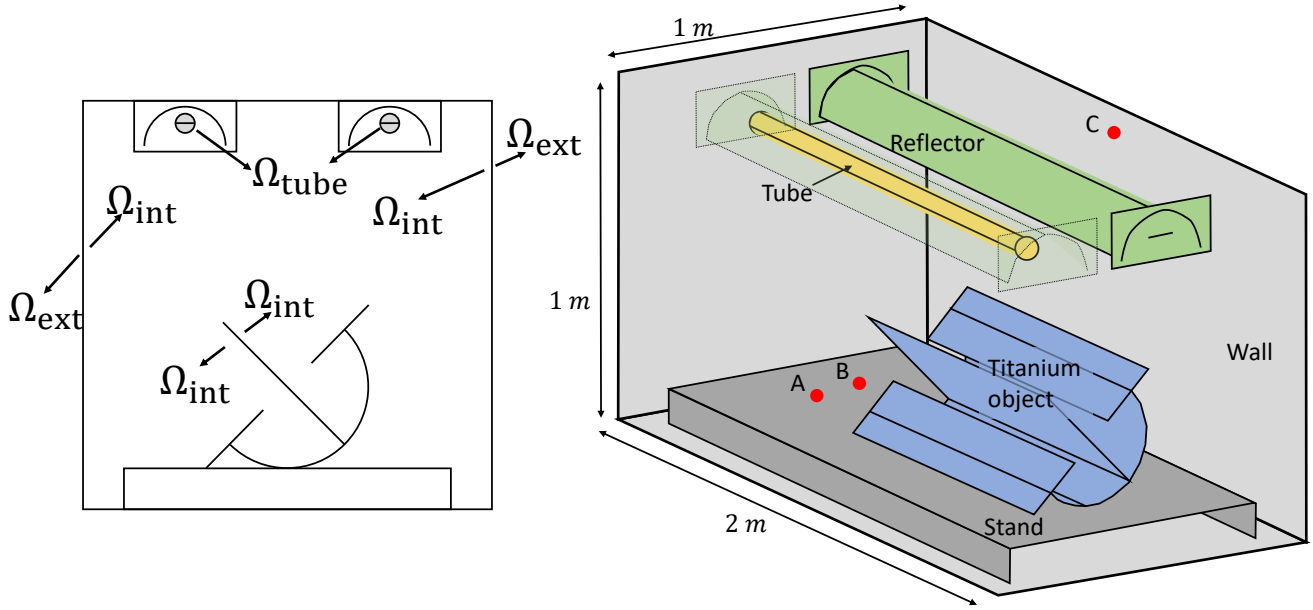


Figure 1: The considered geometry

of the global heat exchange coefficient with the surroundings $h_{ext} = 1\,W.m^{-2}.K^{-1}$. The outside temperature is supposed to be constant at $T_{ext} = 293.15K$. The convective exchanges between the indoor surfaces $\Omega_{int}$ of the furnace are represented by a constant coefficient $h_{int} = 5\,W.m^{-2}.K^{-1}$ and a fluid temperature $T_{int}(T)$ that depends on the temperature of all internal surfaces. Assuming that the heat capacity of the internal fluid is negligible compared to that of the walls, a simple heat balance provides the expression of indoor temperature:

$$T_{int}(T) = \frac{\int\limits_{\Omega_{int}} h_{int}\, T\, d\Omega}{\int\limits_{\Omega_{int}} h_{int}\, d\Omega}\,. \tag{1}$$

Two radiant tubes dissipate an infra-red radiative heat flux. The power radiated by each tube is driven by the temperature $T_{gas}(t)$ of their intern gas whose value depends on time. The heat exchange between the gas and the tube walls $\Omega_{tube}$ is modeled by a global heat exchange coefficient $h_{gas} = 10,000\,W.m^{-2}.K^{-1}$. Then, the tube walls heat by radiation a titanium object with a complex shape placed on a stand. The different thermophysical properties of these elements are given in Table 1. In this first study, they are considered constant .

The objective of this study is to recover the temperature of the gas inside the radiant tube from temperature measurements on easily accessible points. Once the heat source has been identified, the whole temperature field of the titanium object can be retrieved. Whatever the temporal scenario of the temperature of the tubes, the initial temperature is $T_0 = 293.15K$, and the heating of the furnace lasts $5 \times 10^4\,s$. The intrinsic difficulty of inverse problem is deepen by the high temperature

| | Heat capacity $c\,[J.m^{-3}.K^{-1}]$ | Thermal conductivity $k\,[W.m^{-1}.K^{-1}]$ | Emissivity $\varepsilon$ | Thickness $e\,[m]$ |
|---|---|---|---|---|
| Object | $2.35 \times 10^6$ | 21.9 | 0.8 | 0.001 |
| Stand | $3.95 \times 10^6$ | 16.3 | 0.95 | 0.005 |
| Wall | $0.18 \times 10^6$ | 45 | 0.95 | 0.01 |
| Tube | $3.4 \times 10^6$ | 45 | 0.95 | 0.01 |
| Reflector | $3.95 \times 10^6$ | 16.3 | 0.3 | 0.001 |

Table 1: Thermophysical characteristics of the different components

range, as each surface inside the furnace radiates towards every other surfaces.

### *2.2. Mathematical model*

#### *2.2.1. Radiative heat flux*

Given the high temperature level, heat exchange by radiation is preponderant. It is modelled by the radiosity method [29, 30]. The considered surface is first discretized in $N_p$ elementary surfaces $\Omega_j^e$, on which the radiative flux is considered constant, $\varphi_{rad} = \overline{\varphi}_j$. These elementary surfaces are named 'patches'. The radiosity method relates the mean flux $\overline{\varphi}_i$ exchanged by patch $\Omega_i^e$ to the set of mean temperatures $\overline{T}_j$, with $j \in [1, N_p]$ :

$$\forall j \in [1, N_p] \quad \sum_{i=1}^{N_p} \left[ \frac{\delta_{ji}}{\varepsilon_i} - \left( \frac{1}{\varepsilon_i} - 1 \right) F_{ji} \right] \overline{\varphi}_i = - \sum_{i=1}^{N_p} \left( \delta_{ji} - F_{ji} \right) \sigma \overline{T}_i^4 \,, \tag{2}$$

where $\delta_{ji}$ is the Kronecker delta and $F_{ji}$ are the view factors. This sign convention ensures that exchanged flux $\overline{\varphi}_i$ is negative if the surface $i$ emits more flux than it absorbs. Relation (2) can be written in matrix form :

$$\mathbf{A}\,\overline{\varphi} = \mathbf{B}\,\overline{\mathbf{T}}^{\mathbf{4}} \,. \tag{3}$$

The mean flux exchanged by a patch $\overline{\varphi}_j$ expresses as:

$$\overline{\varphi}_j = \sum_{i=1}^{N_p} r_{ji} \overline{T}_i^4 \,, \tag{4}$$

where $r_{ji}$ are the elements of $\mathbf{R}_{rad}\,[N_p,\, N_p] = \mathbf{A}^{-1}\,\mathbf{B}$.

#### *2.2.2. Variational Formulation*

Considering the thinness of the walls and different objects, the Biot number is very small, and the temperature gradient in the thickness is neglected. A shell model can be used, as in references

[25, 28], and its weak formulation is written as :

$$\int_{\Omega} e\,c\frac{\partial T}{\partial t} f\,d\Omega = -\int_{\Omega} e\,k\,\underline{\nabla} T\cdot\underline{\nabla} f\,d\Omega + \int_{\Omega_{int}} \varphi\,f\,d\Omega + \int_{\Omega_{ext}} \varphi\,f\,d\Omega + \int_{\Omega_{tube}} \varphi\,f\,d\Omega\,, \tag{5}$$

where $f \in H^1(\Omega)$ is the test function of the variational formulation on surface $\Omega$, $e$ is the thickness, $c$ thermal heat capacity and $k$ the thermal conductivity. Surfaces $\Omega_{ext}$, $\Omega_{int}$ and $\Omega_{tube}$ of domain $\Omega$ are represented in Figure 1. $\varphi$ is the heat flux exchanged by convection and radiation, and is expressed as :

$$\forall T \in \Omega, \quad \varphi = h(T_f - T) + \overline{\varphi}, \tag{6}$$

with $T_f$ the temperature of the surrounding fluid and $h$ the associated heat exchanged coefficient.

The variational formulation finally reads as :

find $T \in H^1(\Omega)$ such that $\forall f \in H^1(\Omega)$,

$$\begin{aligned}\int_{\Omega} e\,c\frac{\partial T}{\partial t} f\,d\Omega = &-\int_{\Omega} e\,k\,\underline{\nabla} T\cdot\underline{\nabla} f\,d\Omega \\ &-\int_{\Omega_{int}} h_{int} T\,f\,d\Omega - \int_{\Omega_{ext}} h_{ext}\,T\,f\,d\Omega - \int_{\Omega_{tube}} h_{gas}\,T\,f\,d\Omega \\ &+\int_{\Omega_{int}} h_{int}\,T_{int}(T)\,f\,d\Omega + \int_{\Omega_{ext}} h_{ext}\,T_{ext}\,f\,d\Omega \\ &+\sum_{j=1}^{N_p}\sum_{i=1}^{N_p}\left(r_{ji}\overline{T}_i^4\right)\int_{\Omega_j^e} f\,d\Omega \\ &+T_{gas}(t)\int_{\Omega_{tube}} h_{gas}\,f,d\Omega\ ,\end{aligned} \tag{7}$$

After spatial discretization, a matrix formulation of Eq. (7) is obtained:

$$\mathbf{C}\frac{d\mathbf{T}}{dt} = [\mathbf{K}+\mathbf{H}]\,\mathbf{T} + \mathbf{U_{cpl}}\,T_{int}\,(\mathbf{T}) + \mathbf{U_0} + \overline{\mathbf{R}}_{rad}\overline{\mathbf{T}}^4 + T_{gas}(t)\ \mathbf{U_{tube}}\,. \tag{8}$$

In this equation:

- Vector $\mathbf{T}$ contains the temperature value at the $N$ discretization points.
- $\mathbf{C}$, $\mathbf{K}$ and $\mathbf{H}$ are $[N \times N]$ symmetric sparse matrices: $\mathbf{C}$ is the thermal inertia matrix, $\mathbf{K}$ the conductivity matrix and $\mathbf{H}$ gathers the different convection terms on $\Omega_{ext}$, $\Omega_{int}$ and $\Omega_{tube}$.

- Vector $\mathbf{U_0}$ corresponds to the external known solicitations and $\mathbf{U_{cpl}}$ represents the convective exchange with the air inside the furnace, at temperature $T_{int}(\mathbf{T})$. This last term is computed thanks to the discretization of Eq. (1):

$$T_{int}(\mathbf{T}) = \mathbf{D}\,\mathbf{T}\,. \tag{9}$$

- Vector $\overline{\mathbf{T}}^4$ of dimension $[N_p]$ contains mean temperatures of every patch $\Omega_i^e$. Radiation matrix $\overline{\mathbf{R}}_{rad}$ $[N \times N_p]$ allots the mean heat flux density from the $N_p$ patches to the $N$ nodes.

$$\overline{\mathbf{T}} = \mathbf{U_R}\,\mathbf{T}\,, \tag{10}$$

- Finally, vector $\mathbf{U_{tube}}$ of dimension $[N]$ stands for the heat source generated by the gas combustion inside the radiant tubes.

The whole thermal scene can be retrieved by solving the set of equations (8), (9) and (10) for a given gas temperature $T_{gas}$. These equations can also be employed in an iterative process to identify $T_{gas}$ from the temperature measurement on a few accessible points. However, considering the size of the matrix problem but mostly the radiative term, the duration of this computation is not compatible with an on-line monitoring objective. The key would be to replace this large size model by a reduced one, able to reproduce the physics in its complexity but with short computation times.

## 3. Reduced Modal Model

### *3.1. Principle*

Modal methods are based on the projection of the temperature on a limited number $\widetilde{N}$ of known spatial functions $\widetilde{V}_i(M)$

$$T(M,t) \approx \widetilde{T}(M,t) = \sum_{i=1}^{\widetilde{N}} \widetilde{x}_i(t)\ \widetilde{V}_i(M)\,. \tag{11}$$

Excitation states $x_i(t)$ become the unknowns of the problem. Following that principle, AROMM method is based on two steps, briefly presented here (details are found in [23] and [28]).

- A modal base composed of $N$ modes $V_i(M)$ is computed. In this study, modes are solution of the Neumann eigenvalue problem :

$$-\int_\Omega e\ k\ \underline{\nabla} V_i \cdot \underline{\nabla} f\ d\Omega = z_i \int_\Omega e\ c\ V_i\ f\, d\Omega\,, \tag{12}$$

where $z_i$ is the eigenvalue associated to eigenmode $V_i$. The characteristic time associated to mode $i$ is defined as $\tau_i = -\frac{1}{z_i}$. It represents the ability of a mode to reproduce a fast dynamic.

- The reduction step is performed by the amalgam method [23]. In this method, dominant modes $V_{i,0}$ are selected among the initial modes. The remaining modes, called minors (noted $V_{i,p}$), are aggregated to the dominant ones, instead of being discarded. The resulting reduced modes, named amalgamated modes, are then a linear combination of the original modes:

$$\forall i \in \left\{1, ...\widetilde{N}\right\} \quad \widetilde{V}_i(M) = V_{i,0}(M) + \sum_{p=1}^{N_i} \alpha_{i,p}\, V_{i,p}(M)\,. \tag{13}$$

The distribution of the original modes $V_i$ in the reduced basis $\widetilde{V}_i$, and the determination of the weighting coefficient $\alpha_{i,p}$ are obtained by minimizing in the modal space an energy criteria based on a given thermal field evolution $T_{ref}(t, M)$ called the reference simulation. However the characteristic time associated to an amalgamated mode is the one of its dominant mode. The reduction process inhibits the responses to fast dynamics.

### *3.2. Reduced modal formulation*

State equations are deduced from the variational formulation (7) : Temperature is replaced by its modal decomposition (11), while test functions $f$ are replaced by the reduced modes $\widetilde{V}_i(M)$. The following system of coupled ordinary differential equations is obtained :
$\forall p, q \in [1, \widetilde{N}]$

$$\begin{aligned}
&\sum_{p=1}^{\widetilde{N}} \frac{\partial \widetilde{x}_p}{\partial t} \int_{\Omega} e\, c \widetilde{V}_p\, \widetilde{V}_q\, d\Omega \\
&\quad = -\sum_{p=1}^{\widetilde{N}} \widetilde{x}_p \int_{\Omega} e\, k\, \underline{\nabla} \widetilde{V}_p \cdot \underline{\nabla} \widetilde{V}_q \; d\Omega \\
&\quad - \sum_{p=1}^{\widetilde{N}} \widetilde{x}_p \left( \int_{\Omega_{int}} h_{int} \widetilde{V}_p\, \widetilde{V}_q\, d\Omega + \int_{\Omega_{ext}} h_{ext} \widetilde{V}_p\, \widetilde{V}_q\, d\Omega + \int_{\Omega_{tube}} h_{gas} \widetilde{V}_p\, \widetilde{V}_q\, d\Omega \right) \\
&\quad + \sum_{p=1}^{\widetilde{N}} \int_{\Omega_{int}} h_{int}\, T_{int}\, \widetilde{V}_q\, d\Omega + \sum_{p=1}^{\widetilde{N}} \int_{\Omega_{ext}} h_{ext}\, T_{ext}\, \widetilde{V}_q\, d\Omega \\
&\quad + \sum_{p=1}^{\widetilde{N}} \sum_{j=1}^{N_p} \sum_{i=1}^{N_p} \left( r_{ji} \overline{T}_i^4 \right) \int_{\Omega_j^e} \widetilde{V}_q\, d\Omega \\
&\quad + T_{gas}(t) \sum_{p=1}^{\widetilde{N}} \int_{\Omega_{tube}} h_{gas}\, \widetilde{V}_q\, d\Omega\,.
\end{aligned} \tag{14}$$

In these equations, indoor temperature $T_{int}$ and the $N_p$ mean temperatures $\overline{T}_i$ are also expressed under modal formulation :

$$T_{int} = \frac{\sum_{i=1}^{\widetilde{N}} \widetilde{x}_i \int_{\Omega_{int}} h_{int}\, \widetilde{V}_i d\Omega}{\int_{\Omega_{int}} h_{int}\, d\Omega} \quad , \quad \overline{T}_i = \frac{\sum_{j=1}^{\widetilde{N}} \widetilde{x}_j \int_{\Omega_i^e} \widetilde{V}_j d\Omega}{\int_{\Omega_i^e} d\Omega} \, . \tag{15}$$

After spatial discretization, a matrix formulation of Eqs. (14) and (15) is obtained :

$$\begin{aligned} \mathbf{L}\,\frac{d\widetilde{\mathbf{X}}}{dt} = \; & (\mathbf{M_K} + \mathbf{M_H})\;\widetilde{\mathbf{X}} + \mathbf{N_0} \\ & + \overline{\mathbf{M}}_{rad}\,\overline{\mathbf{T}}^4 + T_{gas}(t)\;\mathbf{N_{tube}}\;, \end{aligned} \tag{16}$$

$$\overline{\mathbf{T}} = \mathbf{U_R}\,\widetilde{\mathbf{V}}\,\widetilde{\mathbf{X}}\,, \tag{17}$$

- Matrix $\widetilde{\mathbf{V}}$ $[N, \widetilde{N}]$ gathers reduced vectors $\widetilde{V}_i$.
- Matrices $\mathbf{L} = \widetilde{\mathbf{V}}^T\,\mathbf{C}\,\widetilde{\mathbf{V}}$, $\mathbf{M_K} = \widetilde{\mathbf{V}}^T\,\mathbf{K}\,\widetilde{\mathbf{V}}$, and $\mathbf{M_H} = \widetilde{\mathbf{V}}^T\,(\mathbf{H} + \mathbf{U_{cpl}}\,\mathbf{D})\;\widetilde{\mathbf{V}}$ are dense matrices of reduced dimension $[\widetilde{N}, \widetilde{N}]$, while matrix $\overline{\mathbf{M}}_{rad} = \widetilde{\mathbf{V}}^T\,\overline{\mathbf{R}}_{rad}$ is of dimension $[N_{patch}, \widetilde{N}]$. This last matrix is not fully reduced as it involves radiative exchange between patches
- Reduced vectors $\mathbf{N_0} = \widetilde{\mathbf{V}}^T\,\mathbf{U_0}$ and $\mathbf{N_{tube}} = \widetilde{\mathbf{V}}^T\,\mathbf{U_{tube}}$ are of dimension $[\widetilde{N}]$.

Equations (16)-(17) are evolved in time by a first-order backward Euler scheme with constant time steps. The reduction of the dimensions of the matrices is accompanied by a swift resolution of the initial thermal problem. The resulting temperature $\widetilde{\mathbf{T}}$ field is easily retrieved from the excitation states:

$$\widetilde{\mathbf{T}} = \widetilde{\mathbf{V}}\,\widetilde{\mathbf{X}} \tag{18}$$

Obviously, computation time and precision depend on the reduction order $\widetilde{N}$. All these functions (Finite Element and AROMM method) are programmed in a homemade code in C ++.

### *3.3. Results*

Geometry depicted in Fig. 1 is first discretized on a P1 finite element mesh. It consists of $N = 12,167$ nodes forming $24,202$ triangle elements and $44,838$ patches for radiation[1]. A complete base $V_i,\ i \in [1,\ N]$ is computed from Eq. (12). The reduced base $\widetilde{V}_j,\ j \in [1,\ \widetilde{N}]$ (Eq. (13)) is then synthesized from the following reference problem:

[1] All calculations were performed on a laptop with a 6-core Intel® Xeon® E-2176M @2.7GHz and 64GB of RAM.

- all surfaces are assumed black bodies $\varepsilon = 1$,
- gas temperature into the radiant tubes is fixed at $T_{gas} = 973.15K$,
- the duration of the process is short $\tau = 120\,s$.

The resulting reduced model is now utilized to perform another simulation, characterized by the following parameters :

- surfaces are now diffuse gray bodies (see Table 1 for emissivity values)
- gas temperature is increased to $T_{gas} = 1273K$,
- the duration process is also increased $\tau = 5 \times 10^4 s$, which corresponds to the time needed to reach the steady state.

The ensuing temperatures are compared to the ones obtained from Eqs. (8) to (10). To quantify the accuracy of the reduced model, the following quantities are defined :

$$\sigma_{max} = \max_{t,\Omega} |T - \widetilde{T}| \quad , \quad \varepsilon_{max} = \frac{\max\limits_{t,\Omega} |T - \widetilde{T}|}{\max\limits_{t,\Omega}(T) - \min\limits_{t,\Omega}(T)} \quad , \quad \overline{\sigma} = \frac{1}{V}\frac{1}{\tau}\int_0^{\Omega}\int_0^{\tau} |T - \widetilde{T}|\, dt\, d\Omega \qquad (19)$$

Domain $\Omega$ corresponds either to the whole thermal scene, or is restricted to the object placed on the stand. Results are presented in Table 2 for several order of reduction.

| | Full scene | | | Heated object | | | | |
|---|---|---|---|---|---|---|---|---|
| $\widetilde{N}$ | $\sigma_{max}$ (K) | $\varepsilon_{max}(\%)$ | $\bar{\sigma}$ (K) | $\sigma_{max}$ (K) | $\varepsilon_{max}(\%)$ | $\bar{\sigma}$ (K) | $t_{CPU}$(s) | Gain |
| 20 | 98.64 | 10.0 | 3.31 | 84.30 | 8.9 | 2.69 | 10 | $\times$2138 |
| 50 | 83.92 | 8.6 | 1.15 | 66.91 | 7.1 | 1.18 | 30 | $\times$712 |
| 100 | 66.58 | 6.8 | 0.73 | 39.38 | 4.2 | 0.95 | 62 | $\times$345 |
| 150 | 74.24 | 7.6 | 0.65 | 33.37 | 3.5 | 0.73 | 95 | $\times$225 |
| 200 | 34.26 | 3.4 | 0.52 | 31.89 | 3.4 | 0.62 | 127 | $\times$168 |
| 300 | 24.59 | 2.5 | 0.35 | 21.49 | 2.3 | 0.48 | 200 | $\times$107 |

Table 2: Efficiency of reduced models

Obviously, as accuracy and computation time increase with the reduction order, this latter is a compromise that depends on the objective :

- the inverse procedure is particularly greedy in terms of computation time, but necessitates a good accuracy only at the measurement points : a low order model is chosen in order to comply with the on-line objective,

- for the unique simulation allowing to recover the thermal field, the reduction order might be increased to improve the precision.

The massive gain in computation time has been achieved only because heavy calculations have been conducted off-line :

- computation linked to radiation
  - view factors $F_{ij}$ : $t_{CPU} \approx 1h$,
  - inversion of the radiosity matrix : $t_{CPU} \approx 8h$,
- construction of the reduced model (full base computation, reference solution and amalgam procedure) : $t_{CPU} \approx 7mn$.

## 4. Inverse problem

### *4.1. General procedure*

The purpose of this study is to retrieve the time evolution of the gas temperature inside the radiant panel $T_{gas}(t)$ from temperature measurements at $N_{mes}$ points located on the furnace. The procedure is schematized by Fig. 2. Measurements are gathered in the data matrix $\mathbf{Y}$. From an initial guessed input value $\widehat{T}_{gas}(t)$, Eq. (16) is solved to get $\widetilde{\mathbf{X}}$. Data are then compared with the outputs of the reduced model $\widehat{\mathbf{Y}}$ :

$$\widehat{\mathbf{Y}} = \mathbf{E}\,\widetilde{\mathbf{V}}\,\widetilde{\mathbf{X}} \tag{20}$$

where $\mathbf{E}$ is a simple boolean matrix called selection matrix. A minimization algorithm procures a new guess for $\widehat{T}_{gas}(t)$, which provides new outputs $\widehat{\mathbf{Y}}$. The iterative procedure is stopped when a criteria is met on the following functional :

$$\mathcal{J}(T_{gas}) = \sum^{N_{pts}} \sum^{N_t} (\mathbf{Y}(t) - \widehat{\mathbf{Y}}(T_{gas}, t))^2 \tag{21}$$

where $N_{pts}$ is the number of measuring points and $N_t$ number of time steps.

The optimization is done through the (*trust-region-reflective*) algorithm implemented in the MATLAB function "*lsqcurvefit*". Trust region algorithms are particularly robust for non convex problems [31] [27].

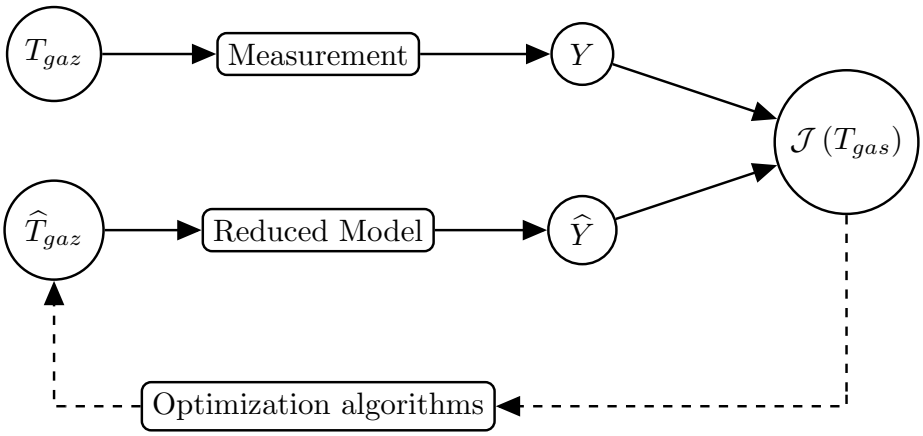


Figure 2: General scheme of the gas temperature estimation by reduced model

*4.2. Data generation*

The present study is fully numeric : temperatures are issued from a finite element simulation, altered with a white noise characterized by a standard deviation $\sigma_N$ of 2 or 5 $K$. The time evolution of temperature $T_{gas}$ is depicted on figure 3. This scenario aggregates several possible types of solicitation : flat levels, linear progression, periodicity. For information, measurement at point A (Fig. 1) with $\sigma_N = 5\,K$ is also represented on Fig. 3. Although the radiative transfer is the main generator, conduction can not be neglected : the temperature response at point A is delayed by about 1000 s compared to $T_{gas}$.

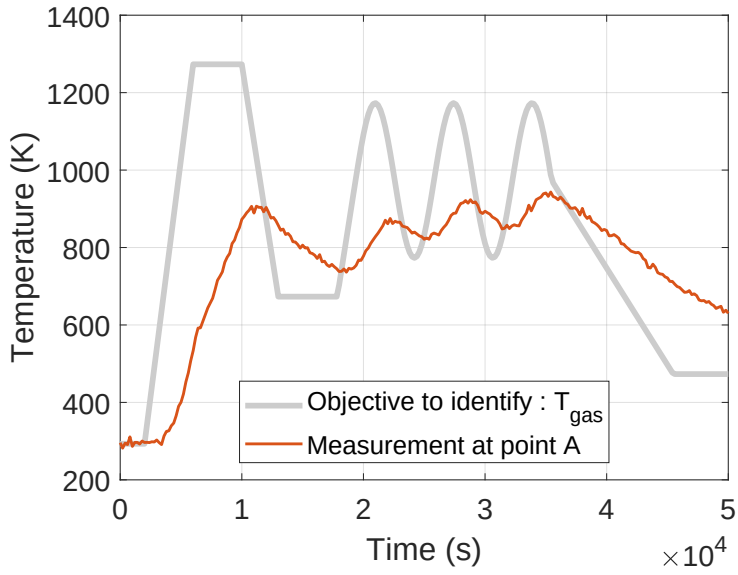


Figure 3: Real temperature $T_{gas}$ and temperature measurement at point A with $\sigma_N = 5$

### *4.3. Radiation sensitivity of reduced model*

Measurement points location is obviously a key parameter for the inverse procedure. Their response to the variation of $T_{gas}$ must be sensitive, while being located on a protected area of the furnace, and not on the heated object itself. The criteria to select the appropriate location is the reduced sensitivity, defined as :

$$S^* = T_{gas} \frac{\partial Y}{\partial T_{gas}} \tag{22}$$

The study has been conducted on the whole possible measurement points, and for three different levels of temperature $T_{gas}$, namely $473\,K$, $673\,K$ and $1273\,K$ (that is to say all the node of Finite Element mesh limited to the stand and walls of the furnace). For clarity, results focus on the 2 most sensitive points for the wall and the stand(respectively points A and C, see Fig. 1).

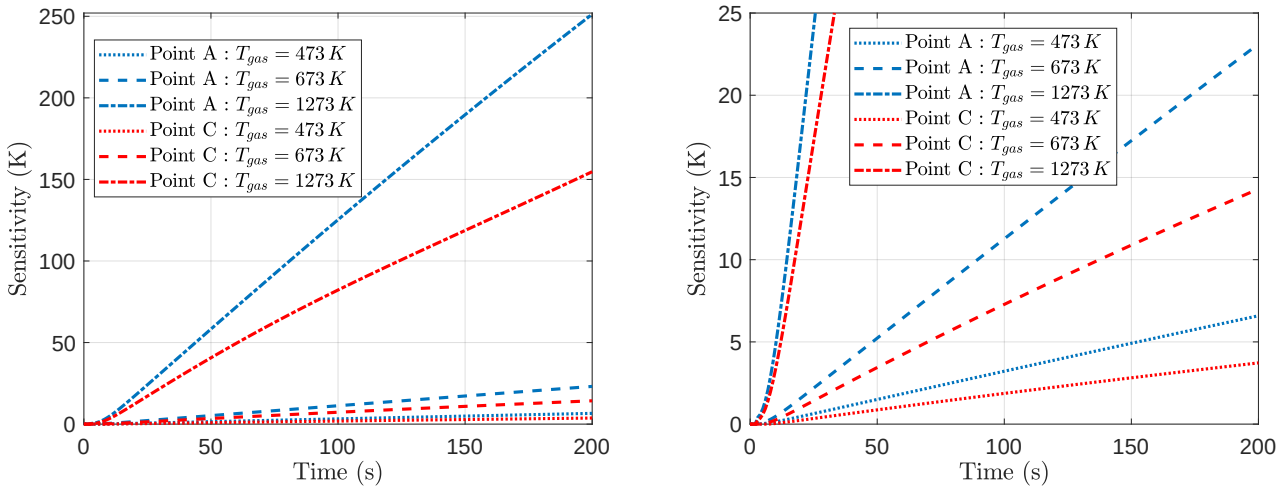


(a) Full scale

(b) Zoom on range $0 - 25K$

Figure 4: Sensitivity study at two measurement points and for different $T_{gas}$ temperature levels

- the non-linear response of the reduced sensitivity towards $T_{gas}$ is clearly evidenced : An increment of 200 K ($473\,K$ to $673\,K$) engenders a sensitivity 2.7 times larger, whereas an increase of 800 K leads to a gain of a factor 40. This illustrates the leading role of radiative heat transfer.

- measurement on the stand leads to a higher sensitivity than on the wall by a ratio 1.6. Therefore points A and B are selected.

- determination of data acquisition frequency is delicate, considering the strong dependence of sensitivity to $T_{gas}$. The acquisition period is fixed to 200 s. For the lower temperature level, this implies a sensitivity of 6.5 K, which is lightly above the standard deviation of the measurement white noise (chosen between 2 and 5 K).

The error induced by the reduction should not exceed the measurement noise, especially at the measurement points. For points A and B, the following quadratic error is defined as:

$$\sigma_{MSE}^{A,B} = \sqrt{\frac{\mathcal{J}(T_{gas})}{N_{pts}\, N_t}} \tag{23}$$

For the validation simulation (see Table 2), and for a reduced model characterized by $\widetilde{N} = 20$, $\sigma_{MSE}^{A,B} = 1.7\,K$ and for a more precise model $\widetilde{N} = 50$, $\sigma_{MSE}^{A,B} = 0.5\,K$. Both models comply with the specifications : a computation time compatible with on-line identification and an error below the measurement noise.

### *4.4. Identification strategy with a time window of variable size*

Temperature value at each time steps has to be identified, which leads to a insurmountable number of parameters (*i.e.* 250) if done at once. Furthermore, one has to wait until the end of the process to start the identification which is clearly out of scope for an on-line identification. Thus, the identification procedure is based on previous works (see Carmona *et al.* [32]) and uses sliding time windows. The size of the window should be large enough to contain sufficient data to permit an accurate identification. On the other hand, the larger the window, the larger the number of parameter to be identified, and thus the longer the computation time. Since the accuracy on the identified variable grows with the size of the time window, this size has to be be adapted to the computation time of the identification process. To conciliate quick start and accuracy, a more elaborate identification strategy is imagined, in which the size of the time window is variable.

Fig. 5 illustrates this strategy, whose outcomes are represented on Fig. 6 (in this last figure, Fig. 6(a) to (d) focused on the initialization phase):

- Phase 1: the first step corresponds to a small time window ($\Delta T_{ident} = 1\,000\,s$ *i.e.* 5 measurement time steps). With this first step, the estimate of the gas temperature is coarse, but is within 20% (Fig. 6 (a)).
- Phase 2: For the following steps, the time identification window grows linearly from 1000 s to 3000 s. Since the data is enriched at each of these steps, the first results quickly obtained at the end of the first 1000 seconds of the process are refined over time (Fig. 6 (b) and (c)). It is noticed that the estimate at the final step of the different window is inaccurate.
- Phase 3: As the maximum size of the window is reached, the sliding begins, with a delay of 200 s (Fig. 6 (d) to (f)). As the objective is to have an on-line identified temperature, the identification process is stopped after 200 s of computation (corresponding to the acquisition period), whatever the degree of convergence.

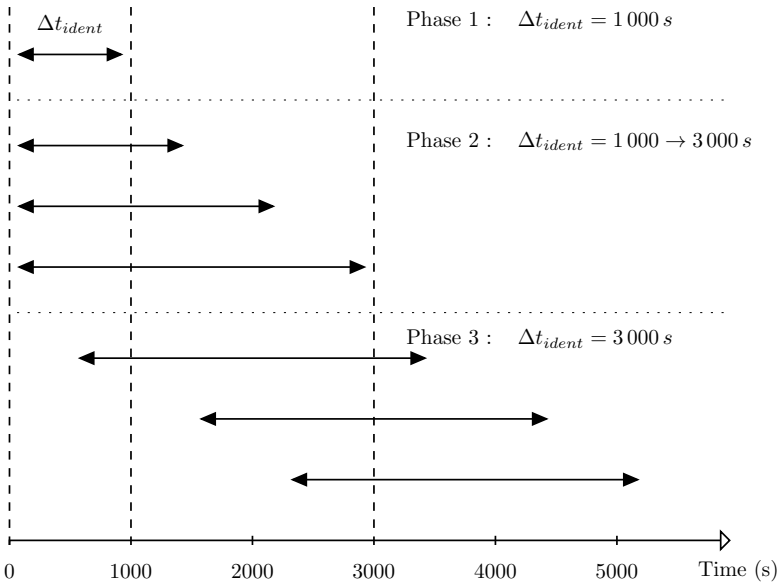


Figure 5: Identification strategy with a variable size window

## 5. Results

### 5.1. Identification of $T_{gas}$

The identification procedure is executed for a first case characterized by a reduced model of order $\widetilde{N}_{(id)} = 20$, and a measurement noise of $\sigma_N = 2\,K$. Figure 6 depicts the identification results over time. Results are very satisfying, as the time evolution is retrieved with a maximum error about 10%. At the beginning of the process, the radiant temperature is low ($293.15\,K$), and so is the sensitivity. This explains the relative inaccuracy at the first $2000\,s$. For a better visualization of the identification procedure, a video animation is procured with the Supplemental Data available online (Identification $\widetilde{N}_{(id)} = 20$ $\sigma_N = 2\,K$).

The impact of the reduction order $\widetilde{N}_{(id)}$ and the measurement noise $\sigma_N$ is studied. To quantify the results, the following quantities are defined:

$$\sigma_{max}^{T_{gas}} = \max_t \left| T_{gas} - \widehat{T}_{gas} \right| \quad , \quad \varepsilon_{max}^{T_{gas}} = \frac{\max\limits_t \left| T_{gas} - \widehat{T}_{gas} \right|}{\max\limits_t (T_{gas}) - \min\limits_t (\widehat{T}_{gas})} \tag{24}$$

$$\sigma_{MSE}^{T_{gas}} = \sqrt{\frac{1}{\tau} \int_0^\tau \left( T_{gas} - \widehat{T}_{gas} \right)^2 dt} \quad , \quad \varepsilon_{MSE}^{T_{gas}} = \frac{\sqrt{\frac{1}{\tau} \int_0^\tau \left( T_{gas} - \widehat{T}_{gas} \right)^2 dt}}{\max\limits_t (T_{gas}) - \min\limits_t (\widehat{T}_{gas})} \tag{25}$$

Table 3 summarizes these errors as well as the CPU times required to solve the inverse problem. Whatever the chosen parameters, results are satisfying as quadratic relative errors $\varepsilon_{MSE}^{T_{gas}}$ stays below 5% while computation time is below the process duration of $50 \times 10^4\, s$. As expected, the errors increases with the measurement noise. However, the accuracy degrades as the order of the reduced model grows, especially on the maximum error $\varepsilon_{max}^{T_{gas}}$, which is counter-intuitive. Indeed, two phenomenons are at stake here. Without doubt, the increase of the order engenders a model more representative of the physics, in its geometric and temporal complexity. However, as the order increases, the model is augmented with modes able to respond to fast dynamics. The reduced model will be able to interpret the high frequency measurement noise by spurious oscillations of the radiant temperature. This is exemplified by Fig. 7 which depicts the identified radiant temperature (as well as its error) for two levels of measurement noise and two orders of the reduced model. Preliminary attempts are thus necessary to determine the optimum reduction order, just as, in other context, they are necessary to find out the correct Thikonov regularization parameter.

| RM Order | $\sigma_N$ (K) | $\sigma_{max}^{T_{gas}}$ (K) | $\varepsilon_{max}^{T_{gas}}$ (%) | $\sigma_{MSE}^{T_{gas}}$ (K) | $\varepsilon_{MSE}^{T_{gas}}$ (%) | $t_{CPU}$ (s) |
|---|---|---|---|---|---|---|
| 20 | 2 | 115 | 11.73 | 25.0 | 2.55 | 4,562 |
| 50 | 2 | 191 | 19.49 | 22.4 | 2.29 | 14,490 |
| 20 | 5 | 145 | 14.80 | 36.0 | 3.67 | 3,913 |
| 50 | 5 | 240 | 24.49 | 44.2 | 4.51 | 14,208 |

Table 3: Computation time for identification of $T_{gas}(t)$

From these results, a reduced model of order $\widetilde{N}_{(id)} = 20$ is chosen.

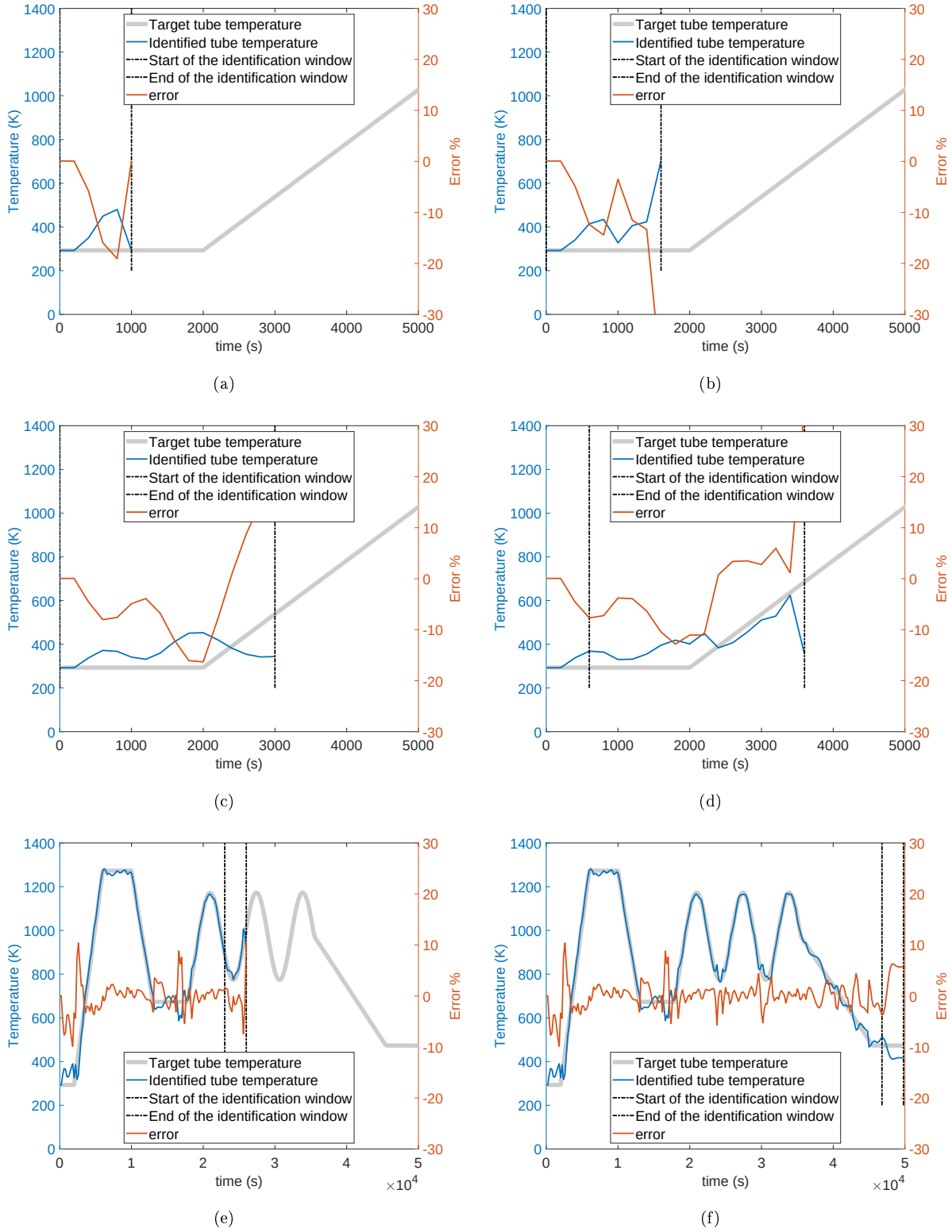


Figure 6: Identification of $T_{gas}$ at different times for a reduced model 20 and $\sigma_N = 2\,K$

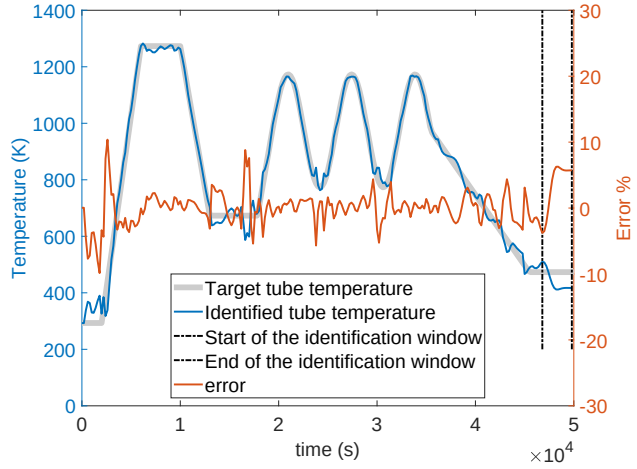


(a) Identification of $T_{gas}$ with 20 modes and noise of $2\,K$

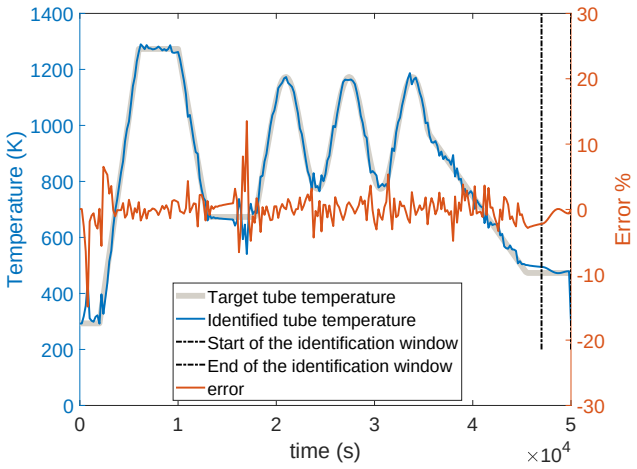


(b) Identification of $T_{gas}$ with 50 modes and noise of $2\,K$

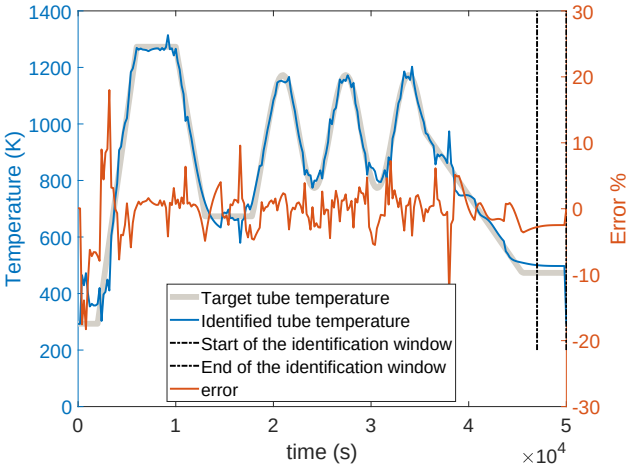


(c) Identification of $T_{gas}$ with 20 modes and noise of $5\,K$

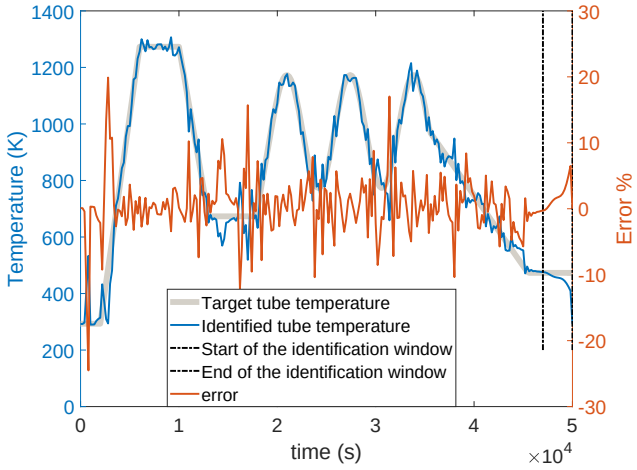


(d) Identification of $T_{gas}$ with 50 modes and noise of $5\,K$

Figure 7: Identification of $T_{gas}$ for different order of reduction and different measurement noise

*5.2. Reconstruction of the thermal field of the piece*

Once the temperature $T_{gas}$ is identified, it can be used as input for a direct simulation to recover the temperature field of the whole thermal scene. As this simulation is done once, a reduced model with a higher order (noted $\widetilde{N}_{(rec)}$) can be used in order to get a more accurate estimation of the temperature. Simulations have been conducted for various order $\widetilde{N}_{(rec)}$ and for several inputs $T_{gas}$ : the exact values, and the identified ones with a measurement noise of $\sigma = 2K$ and $\sigma = 5K$ and $\widetilde{N}_{(id)} = 20$. These results have been compared to those obtained by a finite element simulation with the exact input $T_{gas}$. Figure 8 presents the error $\bar{\sigma}$ (defined by Eq. (19)) localized on the heated object.

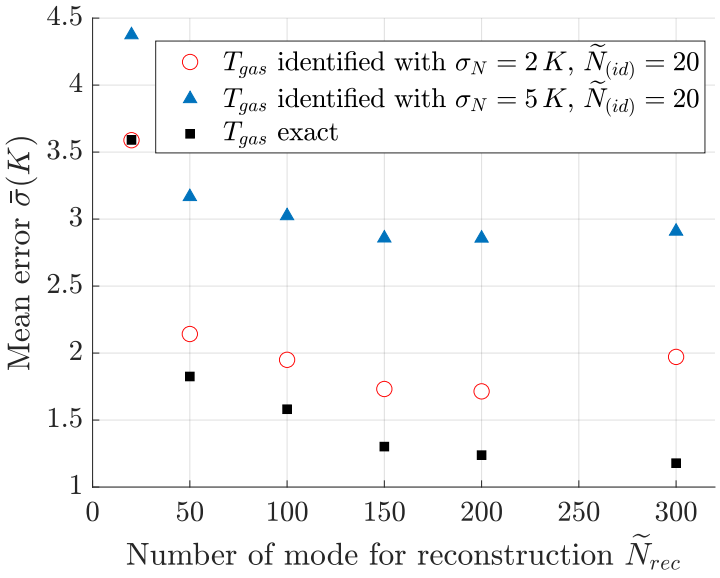


Figure 8: Mean error $\bar{\sigma}$ of reconstruction for the piece with $T_{gas}$ identified ($\widetilde{N}_{(id)}$=20) and real $T_{gas}$

Reduced simulations that use the exact temperature $T_{gas}$ lead to consistent results as the error decreases as the order of the model increases. The magnitude of the errors are in agreement with those indicated in Table 2. Results issued from reduced simulations that use identified temperature need a more refined analysis. The error does not behave monotonously with the reduction order : a minimum appears at $\widetilde{N}_{rec} = 150$. Indeed, reduction acts as a low pass filter. Therefore, a low order reduced model can not respond to the spurious oscillations of the identified temperature. As its order increases, the reduced model becomes more accurate, but also more sensitive to this high frequency fluctuations caused by identification errors.

The noise on the measurement temperature has a notable effect on the recovered temperature field, as the mean error goes from $\bar{\sigma} = 1.75\,K$ for $\sigma_N = 2\,K$ to $\bar{\sigma} = 2.9\,K$ for $\sigma_N = 5\,K$. It is quite noticeable that the mean error committed on the temperature field of the heated object has the same magnitude than the standard deviation of the added noise.

Figure 9 represents temperature and error fields with $\widetilde{N}_{rec} = 150$ modes, for a measurement noise characterized by $\sigma_N = 5\,K$, and at the time where the error is maximum on the heated object (t=6000s). The strong temperature gradient on the contact zone object/stand explains the maximal error of $38\,K$

A direct simulation with a reduced model of order $\widetilde{N}_{rec} = 150$ lasts $0.4\,s$ for each measurement step : the additional cost is negligible, and the reconstruction of the temperature can be implemented in the on-line procedure.

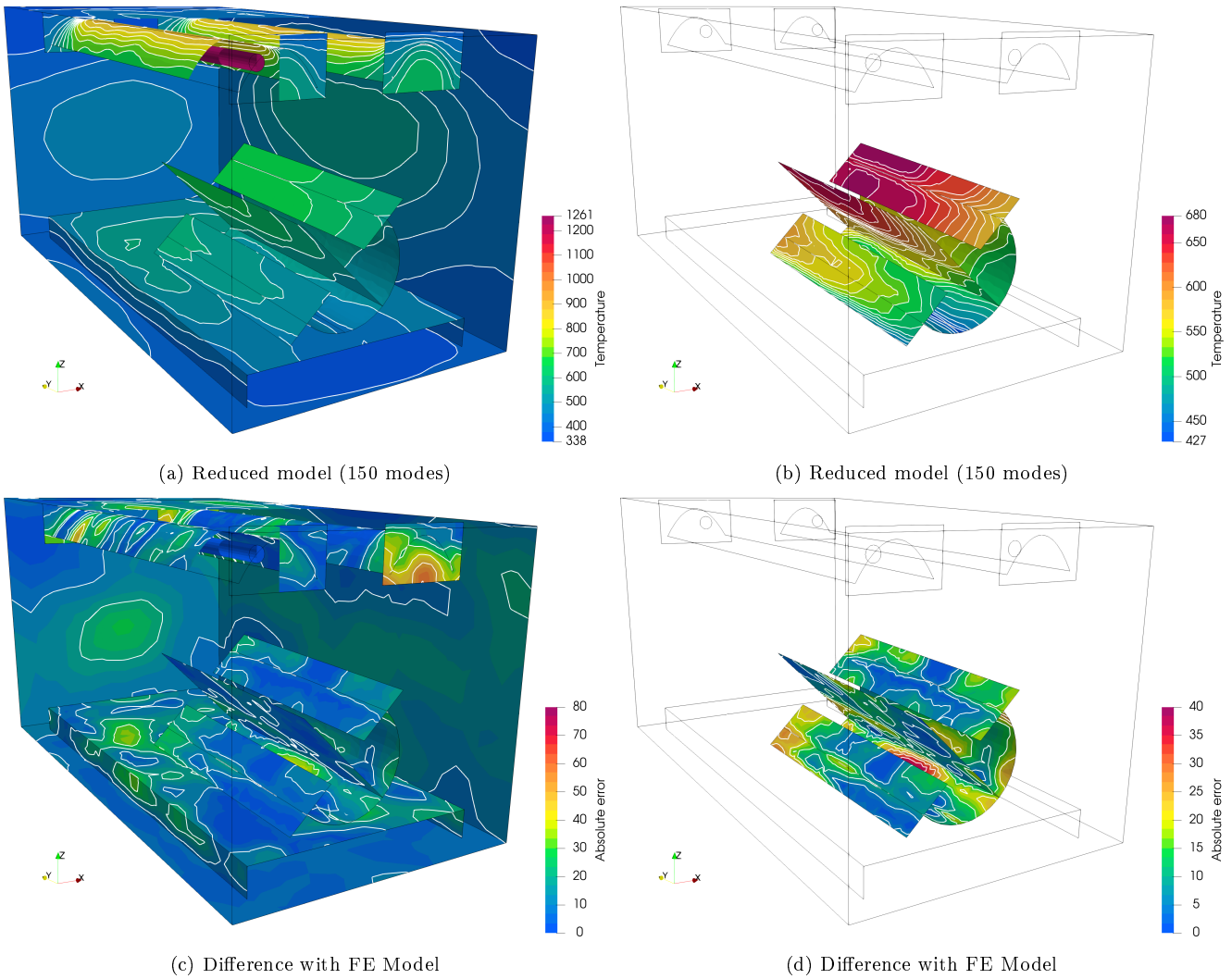


(a) Reduced model (150 modes)

(b) Reduced model (150 modes)

(c) Difference with FE Model

(d) Difference with FE Model

Figure 9: Temperature and error fields at $t = 6\,000\,s$ for reconstruction with $\widetilde{N}_{(rec)} = 150$ modes in the case of identification with $\widetilde{N}_{(id)} = 20$ modes and $\sigma_N = 5\,K$.

## 6. Conclusion

This paper dealt with an object with a complex shape subjected to a heat treatment in an furnace. The objective of this study was to recover on-line the time evolution of the temperature field on the whole object. The main obstacle is the radiative heat transfer, preponderant in this study, which leads to complex numerical models. To overcome this lock, AROMM method has been used to identify the temperature of radiant tubes, but also to recover the temperature field on the whole object.

Regarding the identification phase, the location of the measurement points has been determined from the sensitivity towards the gas temperature. The sensitivity also permits to set the acquisition period. In order to limit the number of parameter to identify, a sliding time window strategy has been adopted : combined with the AROMM method, this strategy enables an on-line identification. The optimum order of the reduced model stays limited to ensure the convergence of the identification procedure in the imposed acquisition period of $200\,s$. In addition, a low order reduced model filters measurement noise and naturally regulates the identified temperature. Other parameters such as thermophysical quantities or convection coefficients are assumed to be well known.

Once the gas temperature has been identified, it has been used as input for a direct simulation to recover the temperature field on the object. A reduced model with a higher reduction order has been used to improve the accuracy. A optimum reduction order appears : it balances the natural increase of the accuracy with the order and the filtering of the spurious oscillations of the identified temperature.

The whole identification procedure lasts less than $5\,000\,s$, which is ten times smaller the duration of the thermal process ($50\,000\,s$). The whole thermal field of the heated object is refreshed every $200\,s$ with an average precision of $\bar{\sigma} = 2.9\,K$, which is below the measurement noise.

This study shows the interest of the AROMM method for an indirect temperature measurement problem in a complex case (complex geometry, radiation). These initial results pave the way to its implementation in a control loop and could be reinforced by including more non-linear parameters and their uncertainties..

## References


[1] K. W. Kim, S. W. Baek, Inverse radiation–conduction design problem in a participating concentric cylindrical medium, International Journal of Heat and Mass Transfer 50 (13) (2007) 2828 – 2837. doi:https://doi.org/10.1016/j.ijheatmasstransfer.2006.10.056.
URL http://www.sciencedirect.com/science/article/pii/S0017931007000518

[2] S. C. Mishra, M. Y. Kim, S. Maruyama, Performance evaluation of four radiative transfer methods in solving multi-dimensional radiation and/or conduction heat transfer problems, International Journal of Heat and Mass Transfer 55 (21) (2012) 5819 – 5835. doi:https://doi.org/10.1016/j.ijheatmasstransfer.2012.05.078.
URL http://www.sciencedirect.com/science/article/pii/S0017931012004073

[3] H. Fan, B. Li, L. Yang, R. Wang, Solution of the inverse radiative load problem in a two-dimensional system, Journal of Quantitative Spectroscopy and Radiative Transfer 74 (1) (2002) 85 – 95. doi:https://doi.org/10.1016/S0022-4073(01)00254-0.
URL http://www.sciencedirect.com/science/article/pii/S0022407301002540

[4] K. Daun, J. Howell, Inverse design methods for radiative transfer systems, Journal of Quantitative Spectroscopy and Radiative Transfer 93 (1) (2005) 43 – 60, fourth International Symposium on Radiative Transfer. doi:https://doi.org/10.1016/j.jqsrt.2004.08.012.
URL http://www.sciencedirect.com/science/article/pii/S0022407304003206

[5] A. Safavinejad, S. Mansouri, A. Sakurai, S. Maruyama, Optimal number and location of heaters in 2-d radiant enclosures composed of specular and diffuse surfaces using micro-genetic algorithm, Applied Thermal Engineering 29 (5) (2009) 1075 – 1085. doi:https://doi.org/10.1016/j.applthermaleng.2008.05.025.
URL http://www.sciencedirect.com/science/article/pii/S1359431108002494

[6] R. Brittes, F. H. França, A hybrid inverse method for the thermal design of radiative heating systems, International Journal of Heat and Mass Transfer 57 (1) (2013) 48 – 57. doi:https://doi.org/10.1016/j.ijheatmasstransfer.2012.09.018.
URL http://www.sciencedirect.com/science/article/pii/S0017931012007120

[7] R. P. Chopade, S. C. Mishra, P. Mahanta, S. Maruyama, Effects of locations of a 3-d design object in a 3-d radiant furnace for prescribed uniform thermal conditions, Applied Thermal Engineering 31 (16) (2011) 3262 – 3274. doi:https://doi.org/10.1016/j.applthermaleng.2011.05.047.
URL http://www.sciencedirect.com/science/article/pii/S1359431111003152

[8] R. P. Chopade, S. C. Mishra, P. Mahanta, S. Maruyama, A. Komiya, Uniform thermal conditions on 3-d object: Optimal power estimation of panel heaters in a 3-d radiant enclosure, International Journal of Thermal Sciences 51 (2012) 63 – 76. doi:https://doi.org/10.1016/

j.ijthermalsci.2011.08.007.
URL http://www.sciencedirect.com/science/article/pii/S1290072911002456

[9] D. Castro, C. Kiyono, E. Silva, Design of radiative enclosures by using topology optimization, International Journal of Heat and Mass Transfer 88 (2015) 880 – 890. doi:https://doi.org/10.1016/j.ijheatmasstransfer.2015.04.077.
URL http://www.sciencedirect.com/science/article/pii/S0017931015004470

[10] A. Farahmand, S. Payan, S. H. Sarvari], Geometric optimization of radiative enclosures using pso algorithm, International Journal of Thermal Sciences 60 (2012) 61 – 69. doi:https://doi.org/10.1016/j.ijthermalsci.2012.04.024.
URL http://www.sciencedirect.com/science/article/pii/S1290072912001482

[11] A. V. Nenarokomov, O. M. Alifanov, I. V. Krainova, D. M. Titov, A. V. Morzhukhina, Estimation of environmental influence on spacecraft materials radiative properties by inverse problems technique, Acta Astronautica 160 (2019) 323 – 330. doi:https://doi.org/10.1016/j.actaastro.2019.04.014.
URL http://www.sciencedirect.com/science/article/pii/S0094576518317235

[12] N. Bayat, S. Mehraban, S. Sarvari, Inverse boundary design of a radiant furnace with diffuse-spectral design surface, International Communications in Heat and Mass Transfer 37 (1) (2010) 103 – 110. doi:https://doi.org/10.1016/j.icheatmasstransfer.2009.07.005.
URL http://www.sciencedirect.com/science/article/pii/S0735193309001742

[13] M. Dashti, A. Mohammad, A. S. O. D. with EGM Approach in Conjugate Natural Convection with Surface Radiation in a Two-Dimensional Enclosure." year =, Optimal design with egm approach in conjugate natural convection with surface radiation in a two-dimensional enclosure.

[14] A. Nenarokomov, O. Alifanov, D. Titov, Space structures insulating material's thermophysical and radiation properties estimation, Acta Astronautica 61 (10) (2007) 873 – 880. doi:https://doi.org/10.1016/j.actaastro.2006.12.023.
URL http://www.sciencedirect.com/science/article/pii/S0094576507001117

[15] M. Dehghani, S. H. Sarvari], H. Ajam, Inverse estimation of boundary conditions on radiant enclosures by temperature measurement on a solid object, International Communications in Heat and Mass Transfer 38 (10) (2011) 1455 – 1462. doi:https://doi.org/10.1016/j.icheatmasstransfer.2011.08.015.
URL http://www.sciencedirect.com/science/article/pii/S0735193311001874

[16] M. Girault, E. Videcoq, D. Petit, Estimation of time-varying heat sources through inversion of a low order model built with the modal identification method from in-situ temperature measurements, Int. J. Heat and Mass Transfer 53 (2010) 206 – 219.

[17] K. Bouderbala, H. Nouira, E. Videcoq, M. Girault, D. Petit, Mim, fem and experimental investigations of the thermal drift in an ultra-high precision set-up for dimensional metrology at the nanometre accuracy level, Applied Thermal Engineering 94 (2016) 491 – 504. doi:https://doi.org/10.1016/j.applthermaleng.2015.09.092.
URL http://www.sciencedirect.com/science/article/pii/S1359431115010170

[18] M. Girault, Y. Liu, Y. Billaud, A. M. Benselama, D. Saury, D. Lemonnier, Reduced order models for conduction and radiation inside semi-transparent media via the modal identification method, International Journal of Heat and Mass Transfer 168 (2021) 120598. doi:https://doi.org/10.1016/j.ijheatmasstransfer.2020.120598.
URL https://www.sciencedirect.com/science/article/pii/S0017931020335341

[19] H. Park, T. Yoon, Solution of the inverse radiation problem using a conjugate gradient method, International Journal of Heat and Mass Transfer 43 (10) (2000) 1767 – 1776. doi:https://doi.org/10.1016/S0017-9310(99)00255-0.
URL http://www.sciencedirect.com/science/article/pii/S0017931099002550

[20] H. Park, M. Sung, Sequential solution of a three-dimensional inverse radiation problem, Computer Methods in Applied Mechanics and Engineering 192 (33) (2003) 3689 – 3704. doi:https://doi.org/10.1016/S0045-7825(03)00370-0.
URL http://www.sciencedirect.com/science/article/pii/S0045782503003700

[21] H. Park, W. Lee, An inverse radiation problem of estimating heat-transfer coefficient in participating media, Chemical Engineering Science 57 (11) (2002) 2007–2014.

[22] R. Hoffmann, A. Seewald, P. Schneider, F. França, Inverse design of thermal systems with spectrally dependent emissivities, International Journal of Heat and Mass Transfer 53 (5) (2010) 931 – 939. doi:https://doi.org/10.1016/j.ijheatmasstransfer.2009.11.030.
URL http://www.sciencedirect.com/science/article/pii/S0017931009006309

[23] A. N. O. Quéméner, F. Joly, The generalized amalgam method for modal reduction, IJHMT 55 (2012) 1197–1207.

[24] S. Grosjean, B. Gaume, F. Joly, K. Vera, A. Neveu, A modal substructuring method for non-conformal mesh. application to an electronic board, International Journal of Thermal Sciences 152 (2020).

[25] S. Carmona, Y. Rouizi, O. Quéméner, F. Joly, A. Neveu, Estimation of heat flux by using reduced model and the adjoint method. application to a brake disc rotating, International Journal of Thermal Sciences 131 (2018) 94 – 104. doi:https://doi.org/10.1016/j.ijthermalsci.2018.04.036.
URL http://www.sciencedirect.com/science/article/pii/S1290072917311171

[26] S. Carmona, Y. Rouizi, O. Quéméner, Spatio-temporal identification of heat flux density using reduced models. application to a brake pad, International Journal of Heat and Mass Transfer 128 (2019) 1048 – 1063. doi:https://doi.org/10.1016/j.ijheatmasstransfer.2018.09.043.
URL http://www.sciencedirect.com/science/article/pii/S001793101831785X

[27] A. C. Castillo, B. Gaume, Y. Rouizi, O. Quéméner, P. Glouannec, Identification of insulating materials thermal properties by inverse method using reduced order model, International Journal of Heat and Mass Transfer 166 (2021) 120683. doi:https://doi.org/10.1016/j.ijheatmasstransfer.2020.120683.
URL https://www.sciencedirect.com/science/article/pii/S001793102033619X

[28] B. Gaume, F. Joly, O. Quéméner, Modal reduction for a problem of heat transfer with radiation in an enclosure, International Journal of Heat and Mass Transfer 141 (2019) 779 – 788. doi:https://doi.org/10.1016/j.ijheatmasstransfer.2019.07.039.
URL http://www.sciencedirect.com/science/article/pii/S0017931019320423

[29] T. Ait-taleb, A. Abdelbaki, Z. Zrikem, Numerical simulation of coupled heat transfers by conduction, natural convection and radiation in hollow structures heated from below or above, Int. J. Therm. Sci. 47 (2008) 378 – 387.

[30] M. A. Antar, Thermal radiation role in conjugate heat transfer across a multiple-cavity building block, Energy 35 (2010) 3508 – 3516.

[31] Y. Li, Centering, trust region, reflective techniques for nonlinear minimization subject to bounds, Technical note, Deptment of Computer Science, Cornell University, Ithaca, NY (1993).
URL https://ecommons.cornell.edu/bitstream/handle/1813/6159/93-1385.pdf?sequence=1&isAllowed=y

[32] S. Carmona, Y. Rouizi, O. Quéméner, F. Joly, A. Neveu, Estimation of heat flux by using reduced model and the adjoint method. application to a brake disc rotating, International Journal of Thermal Sciences 131 (2018) 94 – 104. doi:https://doi.org/10.1016/j.ijthermalsci.2018.04.036.
URL http://www.sciencedirect.com/science/article/pii/S1290072917311171